

APARATE: Adaptive Adversarial Patch for CNN-based Monocular Depth Estimation for Autonomous Navigation

Amira Guesmi¹, Muhammad Abdullah Hanif¹, Ihsen Alouani² and Muhammad Shafique¹

Abstract—In recent years, monocular depth estimation (MDE) has witnessed a substantial performance improvement due to convolutional neural networks (CNNs). However, CNNs are vulnerable to adversarial attacks, which pose serious concerns for safety-critical and security-sensitive systems. Specifically, adversarial attacks can have catastrophic impact on MDE given its importance for scene understanding in applications like autonomous driving and robotic navigation. To physically assess the vulnerability of CNN-based depth prediction methods, recent work tries to design adversarial patches against MDE. However, these methods are not powerful enough to fully fool the vision system in a systemically threatening manner. In fact, their impact is partial and locally limited; they mislead the depth prediction of only the overlapping region with the input image regardless of the target object size, shape and location. In this paper, we investigate MDE vulnerability to adversarial patches in a more comprehensive manner. We propose a novel adaptive adversarial patch (APARATE¹) that is able to selectively jeopardize MDE by either corrupting the estimated distance, or simply manifesting an object as disappeared for the autonomous system. Specifically, APARATE is optimized to be shape and scale-aware, and its impact adapts to the target object instead of being limited to the immediate neighborhood. Our proposed patch achieves more than 14 meters mean depth estimation error, with 99% of the target region being affected. We believe this work highlights the threat of adversarial attacks in the context of MDE, and we hope it would alert the community to the real-life potential harm of this attack and motivate investigating more robust and adaptive defenses for autonomous robots.

Index Terms—Machine Learning Security, Adaptive Adversarial Patch, Physical Adversarial Attacks, Monocular Depth Estimation, Robot Navigation, Autonomous Robots, Autonomous Vehicles.

I. INTRODUCTION

Monocular depth estimation (MDE) is increasingly used in many real-world applications such as robotics and autonomous driving (AD). MDE is used to get depth information from a single image and therefore get a better understanding of the scene. In fact, it is an essential part of many robotic tasks like obstacle avoidance [3], object detection [4], visual SLAM [5], [6], and visual relocalization [7], etc.

Some depth estimation techniques depend on RGB-D cameras, Radar, LiDAR or ultrasound devices to directly get the depth information from a scene, where the latter suffer from serious drawbacks. In fact, RGB-D cameras have

a limited measurement range, LiDAR and Radar produce sparse information and are costly sensors that may not be deployed in small scale autonomous systems, and ultrasound devices suffer from inherently inaccurate measurements. In addition, the above devices are energy-hungry with large sizes, which is unsuitable to small-sized and resource-constrained systems especially those subject to strict real-world design restrictions. On the contrary, RGB cameras are lightweight and cheaper. More importantly, they can provide richer information about the environment.

Leading companies in autonomous vehicles are trying to advance self-driving technology with low-cost cameras. In fact, MDE has been integrated into Tesla’s production-grade Autopilot system [8], [9]. Other AD companies such as Toyota [10] and Huawei [11] are following the lead of Tesla in trying to advance self-driving technology with this technique. This increase in popularity is owed to the employment of Deep learning networks, and since those latter were proven to be vulnerable to adversarial attacks, ensuring MDE models security becomes crucial.

Adversarial attacks for deep learning systems can be categorized into two settings: (1) *digital attacks* [12], [13], where an attacker maliciously adds imperceptible adversarial noise to the digital input image; and (2) *physical attacks* [14]–[17], where the attacker creates and prints an adversarial patch and places it in the scene which will be fed to the victim model through the captured image. In this work, we focus on the second category due to its practical use in real world scenarios against the vision system of an autonomous car or a navigation system of a robot. Physical Adversarial Examples are crafted with the purpose of them being printed out and recaptured by a camera. As a result, the attacker can only control a subset of the pixels that will be fed into the victim model. Moreover, the attacker has no control over perspective, scale, and other processing that cameras perform, making it more challenging since the adversarial examples need to be robust to these various transformations for the attack to succeed in a physical setting. In fact, extending the digital attack to the physical world adds another layer of difficulty, as it requires the perturbation to be robust enough to survive real-world distortions due to different viewing distances and angles, lighting conditions, and camera limitations. These physical world challenges include the environmental conditions, e.g., the distance and the angle of a camera. The fabrication error, all perturbation values must be valid colors that can be reproduced in the real world. Furthermore, even if a fabrication device, such as a printer, can produce certain colors, there will be some

¹Amira Guesmi, Muhammad Abdullah Hanif, and Muhammad Shafique are with eBrain Laboratory, NYU Abu Dhabi, UAE ag9321@nyu.edu

²Ihsen Alouani is with CSIT, Queen’s University Belfast, UK

¹We use the name APARATE, which is a non-verbal transportation spell in Harry Potter movies that allows to instantly travel on the spot and appear at another location.

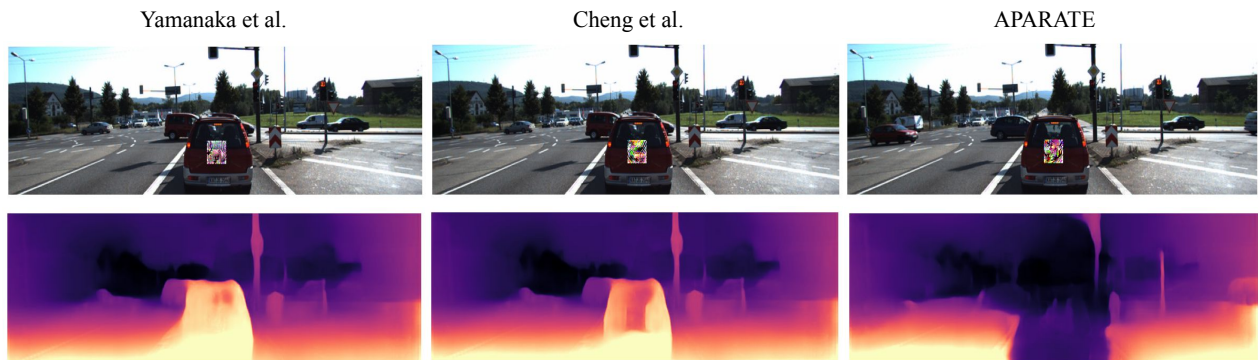


Fig. 1: Our APARATE makes the object fully disappear, in contrast, adversarial patches proposed by Yamanaka et al. [1] and Cheng et al. [2] are weak adversarial patches that only impact the depth of a small region of the target object which is restricted to the overlapping region between the patch and the input image.

reproduction error.

Prior efforts for physical-world adversarial attacks [1], [2] produced weak adversarial patches that only impact the depth of a small region of a target object (e.g., vehicles and pedestrians). The affected area is restricted to the overlapping region between the patch and the input image, leaving plenty of room for improvement. We propose a method for generating adversarial patches for CNN-based monocular depth estimation. Specifically, we generate adversarial patches that can fool the target methods into estimating an incorrect depth of a chosen object (e.g., vehicles, pedestrians) or completely hide that object.

In summary, the novel contributions of this work are:

- We propose a penalized loss function to increase the impact of the patch and enlarge the affected region (see Figure 1).
- Our proposed attack is generic so it can be applied to any class of objects on public roads. This paper focuses on two representative types of objects to attack: cars and pedestrians.
- An automated placement of the patch during the optimization rather than randomly placing it on the scene so the patch won't be trained on irrelevant objects.
- Our proposed patch achieves more than 14 meters mean depth estimation error, with 99% of the target region affected.

Figure 2 presents an overview of our framework, a full description is provided in section II-B.

II. PROPOSED APPROACH

A. Problem formulation

In depth estimation, given a benign image I , the purpose of the adversarial attack is to make the depth estimation method miss-predict the depth of the target object using the maliciously designed image I^* . Technically, the adversarial example with generated patch can be formulated as:

$$I^* = (1 - M_P) \odot I + M_P \odot P \quad (1)$$

\odot is the component-wise multiplication, P is the adversarial patch, and M_P is the patch mask, used to constrict the size, shape, and location of the adversarial patch. The adversarial depth, i.e., the output of the victim model F when taking as input the adversarial example is:

$$d_{adv} = F((1 - M_P) \odot I + M_P \odot P) \quad (2)$$

The problem of generating an adversarial example can be formulated as a constrained optimization 3, given an original input image I and a MDE model $F(\cdot)$:

$$\min_P \|P\|_p \text{ s.t. } F((1 - M_P) \odot I + M_P \odot P) \neq F(I) \quad (3)$$

The objective is to find a minimal adversarial noise, P , such that when placed on an arbitrary object from a target input domain U , it will selectively jeopardize the underlying DNN-based MDE model $F(\cdot)$ by either corrupting the estimated distance, or simply making an object disappear. Note that one cannot find a closed form solution for this optimization problem since the DNN-based model $F(\cdot)$ is a non-convex machine learning model. Therefore, 3 can be formulated as follows to numerically solve the problem using empirical approximation techniques:

$$\arg \max_P \sum_{I \in \mathcal{U}} l(F((1 - M_P) \odot I + M_P \odot P), F(I)) \quad (4)$$

where l is a predefined loss function and $\mathcal{U} \subset U$ is the attacker's training dataset. We can use existing optimization techniques (e.g., Adam [18]) to solve this problem. In each iteration of the training the optimizer updates the adversarial patch P .

B. Overview

For the sake of comparison, we try to replicate the work in [1] where an adversarial patch was trained for random placement on the scene, in contrast, [2] propose a patch trained on the same object for a fixed distance from the camera (we overlook the stealthiness constraint as this is out of the scope of our work). As clearly shown in Figure 1, our patch APARATE completely makes the object disappear, on

the other hand, we notice limited impact for the other two patches. For the comparison, we use the same parameters in optimization with the same patch size and shape.

Our goal in this paper is to generate physical adversarial patches with an impact that covers the whole object regardless of its size, shape, or location, while still maintaining their attack performance. To achieve this, we propose to use a pre-trained object detector to identify the targeted object location (i.e., the object that we seek to hide or change its predicted depth) and by that produce a patch that robust to different distances from the camera. We also propose a new loss function to enhance the impact of the patch and enlarge the affected region.

As illustrated in Figure 2, given a pre-trained object detector we generate two masks: the patch mask (M_p) corresponding to the placement of the patch at the center of the target object and the focus mask (M_f) corresponding to the region covered by the target object, i.e., the target affected region. We feed the patch to the patch transformer and perform the geometric transformations described in Section II-D. We, later on, use the patch applier to render the patch on top of the input image by harnessing information from the object detector as described in section II-C. After that, we perform a forward pass, i.e., we feed the resulting adversarial image to the MDE model. The next step is to apply the generated masks to compute the required loss functions. Then, we compute the gradient of the patch and based on this information we update the patch P .

C. Patch Applier

In a physical attack setting, we can't control the perspective, the scale nor the position of the adversarial patch with respect to the camera. Therefore, to increase the robustness of our patch to a broad range of possibilities, we render this latter on top of the target object (e.g., back of a car or the clothes of humans) and we simulate different scenes at different settings. A number of transformations are included in the optimization process, such as rotation and occlusion in order to simulate how our adversarial patch P may look like in a realistic scenario. Next, we use the object detector to get the correct locations of the object (e.g., cars or persons) in a given image I . We place our adversarial patch P on the detected object. We use the object detector to create a mask around the object that we named M_f and a mask M_p that will constrict the location, the size and the shape of the generated patch. The object detector is only used for the optimization process of the patch and not during the attack itself. To avoid manually placing the patches on the objects, like in [2], we use YOLOv4-tiny [19] object detector pretrained on MSCOCO [20].

Let $U = \{I_i\}_{i=1}^M$ and $V = \{J_j\}_{j=1}^N$ respectively be the M training and N testing images for a particular scene of attack. We run the YOLOv4-tiny object detector on U and V with an objectness threshold of 0.5 and non-max suppression IoU threshold of 0.4. This yields the tuples:

$$T_i^U = \{(B_{i,k}^U)\}_{k=1}^{D_i}, T_j^V = \{(B_{j,l}^V)\}_{l=1}^{E_j} \quad (5)$$

for each I_i and J_j , where D_i is the number of detections in I_i (fixed to 14 in our experiment same as in [21]). and $B_{i,k}^U$ is the bounding box of the k -th detection in I_i . (Same for E_j and $B_{j,l}^V$ for J_j). The sets of all detected objects are:

$$T^U = \{T_i^U\}_{i=1}^M, T^V = \{T_j^V\}_{j=1}^N \quad (6)$$

The information used to optimize P for a scene of attack are the training images U and annotations T^U . The patch P is randomly initialized. Given the current P , the patch is rendered on top of each detected object of the chosen class for each training image I_i using the mask $M_{p_{i,k}}^U \cdot M_{p_{i,k}}^U$ is a matrix of zeros except for the patch location (The center of the patch is the center of the bounding boxes). The focus mask $M_{f_{i,k}}^U$ is defined as the space limited by the generated bounding boxes $B_{i,k}^U$ in a way that it covers the whole detected object. $M_{f_{i,k}}^U$ is a matrix of zeros except for the targeted regions (objects covered area) where the pixel values are ones. We multiply the generated masks with the adversarial depth map d_{adv} and use the resulting maps to compute the two losses.

D. Patch Transformer

The distance and angle of a camera in an autonomous vehicle with respect to another vehicle or any other target object vary continuously. The resulting images that are fed to the victim model are taken at different distances, angles, and lighting conditions. Therefore, any perturbation (i.e., adversarial patch) that an attacker physically adds to the scene must be able to survive these transformations

We use several physical transformations to simulate these dynamic factors. Technically, we take into account the transformations of inclusion of variable conditions, such as adding noise, random rotation, variable scales, lighting variation, etc. The above physical transformation operations are performed using the patch transformer. The geometric transformations applied are: **Random scaling** of the patch to a size that is roughly equivalent to its physical size in the scene. Perform **random rotations** ($\pm 20^\circ$) on the patch P about the center of the bounding boxes $B_{i,k}^U$. The above simulates placement and printing size uncertainties. The color space transformations are done by changing the pixel intensity values by adding **random noise** (± 0.1), performing **random contrast** adjustment of the value ($[0.8, 1.2]$), and **random brightness** adjustment (± 0.1). The resulting image $T_\theta(I_i)$ is forward propagated through the MDE.

E. Penalized Depth Loss

We use the produced bounding boxes $B_{i,k}^U$ to generate a focus mask M_f covering the region whose predicted depth we want to modify. Our goal is to enlarge the area affected by the patch so that it's not just limited to overlapping pixels. We split the L_{depth} into two terms L_{d_1} and L_{d_2} . L_{d_1} is the loss of pixels overlapped by the patch and L_{d_2} is the loss of the non-overlapped pixels. In order to force the optimizer to prioritize the minimization of the non-overlapped pixels loss L_{d_2} , we square the term of the difference between the output depth and the target depth $|d_t - d_{adv}| \odot M_P$, as in

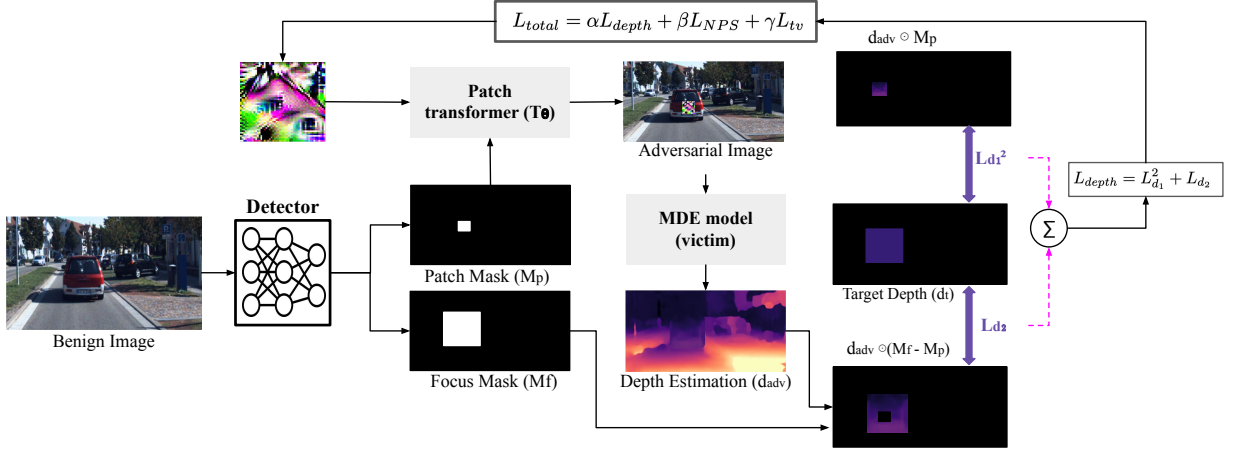


Fig. 2: **Overview of the proposed approach:** Given a pre-trained object detector we generate two masks: the patch mask (M_p) corresponding to the location of the patch at the center of the target object and the focus mask (M_f) corresponding to the object covered area and the attacked region. We feed the patch to the patch transformer and perform the geometric transformations described in Section II-D. We, later on, render the patch on top of the input image by harnessing information from the object detector as described in section II-C. After that, we perform a forward pass, i.e., we feed the resulting adversarial image to the MDE model. The next step is to apply the generated masks to compute the required loss functions. Then, we compute the gradient of the patch and based on this information we update the patch P .

quadratic functions the rate of increase (the slope or the rate of change) is slower which delays the convergence of the overlapped pixels loss vis-a-vis the non-overlapped pixels.

The adversarial losses are defined as the distance between the predicted depth and the target depth and calculated as follows:

$$L_{d_1} = (|d_t - d_{adv}| \odot M_p) \quad (7)$$

$$L_{d_2} = |d_t - d_{adv}| \odot (M_f - M_p) \quad (8)$$

$$L_{depth} = L_{d_1}^2 + L_{d_2} \quad (9)$$

F. Adversarial Patch Generation

We iteratively perform gradient updates on the adversarial patch (P) in the pixel space in a way that optimizes our objective function defined as follows:

$$L_{total} = \alpha L_{depth} + \beta L_{NPS} + \gamma L_{tv} \quad (10)$$

L_{depth} is the adversarial depth loss. L_{NPS} representing the non-printability score. The L_{NPS} term encourages colors in P to be as close as possible to colors that can be reproduced by a printing device.

It is defined as:

$$L_{NPS} = \sum_{i,j} \min_{c \in C} (\| P_{i,j} - c \|_2) \quad (11)$$

where $P_{i,j}$ is the pixel (RGB vector) at (i, j) in P , and c is a color vector from the set of printable colors [22].

where m and n are the image dimensions. L_{tv} is the total variation loss on the generated image to encourage

smoothness. It is defined as:

$$L_{tv} = \sum_{i,j} \sqrt{(P_{i+1,j} - P_{i,j})^2 + (P_{i,j+1} - P_{i,j})^2} \quad (12)$$

where the sub-indices i and j refer to the pixel coordinate of the patch P .

α , β , and γ are hyper-parameters used to scale the three losses. For our experiments, we set $\alpha = 1$, $\beta = 1.5$, and $\gamma = 0.1$. We optimize the total loss using Adam [18] optimizer. We try to minimize the object function L_{total} and optimize the adversarial patch. We freeze all weights and biases in the depth estimator and only update the pixel values of the adversarial patch. The patch is randomly initialized. Algorithm 1 illustrates the different stages described in the above sections in order to train our adversarial patch.

III. EXPERIMENTAL RESULTS

A. Experimental Setup

For our experiments, we use three MDE models: the monodepth2 [23], Depthhints [24], and Manydepth [25]. Three self-supervised depth prediction models chosen based on their practicality and open source codes, same models used in [2]. The three models are based on the general U-Net architecture, i.e. an encoder-decoder network, enabling the representation of both deep abstract features as well as local information. The ResNet18 [26] pretrained on ImageNet [27] was used as the encoder and the decoder was based on several convolution and upsampling layers with skip connections used to decode the output back to the input resolution. We use real-world driving scenes from KITTI 2015 dataset [28] to generate and evaluate the attack performance on different objects. The dataset consists of calibrated stereo video registered to LiDAR measurements of a city, captured

Algorithm 1 APARATE.

```

1: Input: Dataset:  $U$ , MDE model:  $F$ , number of epochs:
    $K$ , clean input:  $I$ , baseline depth  $d$ , adversarial depth
    $d_{adv}$ , object detector:  $D$ 
2: Output:  $P$  adversarial patch.
3: Initialize  $P \leftarrow \text{random}(0, 1)$ 
4: for  $epoch = 0 : K$  do
5:   for  $I$  in  $U$  do
6:      $d = F(I)$ 
7:      $(M_P, M_f) \leftarrow D(\text{data})$ 
8:      $d_{adv} = F((1 - M_P) \odot I + M_P \odot T_\theta(P))$ 
9:      $L_{d_1} = |d_t - d_{adv}| \odot M_P$ 
10:     $L_{d_2} = |d_t - d_{adv}| \odot (M_f - M_P)$ 
11:     $L_{depth} = L_{d_1}^2 + L_{d_2}$ 
12:     $L_{NPS} = \sum_{i,j} \min_{c \in C} (\|P_{i,j} - c\|_2)$ 
13:     $L_{tv} = \sum_{i,j} \sqrt{(P_{i+1,j} - P_{i,j})^2 + (P_{i,j+1} - P_{i,j})^2}$ 
14:     $L_{total} = \alpha L_{depth} + \beta L_{NPS} + \gamma L_{tv}$ 
15:    compute loss backward
16:    perform optimizer step
17:    set the gradient of the optimizer to 0
18:    clamp( $P$ , [0,1])
19:   end for
20: end for

```

from a moving car. The captured scenes cover a wide range of roads (e.g., local/rural roads and high-way) (e.g., vehicles, pedestrians, and traffic lights).

B. Evaluation Metrics

In order to evaluate the performance of our proposed attack, we use two metrics: *the mean depth estimation error* E_d of the target object and *the ratio of the affected region* R_a . We use depth prediction of the benign object as the ground truth and compare with depth prediction of the adversarial object. The mean depth estimation error denotes the attack effectiveness of our proposed patch. The larger it is, the better the performance, same for the R_a metric. We modify the metrics used in [2] to align them with our settings since they are inapplicable to our scenario. In fact, contrary to what is proposed in [2]; where their patch is trained on a single object placed at a fixed distance from the camera and only changing the background, however, we train our patch for different distances (i.e., objects can be at different positions relative to the camera e.g. near, far, left, right or center). We identify objects that are closer to the camera by setting a threshold, we first normalize the output of the disparity map between 0 and 1. let 0 correspond to the farthest point in the image and 1 the closest point. Objects with a normalized disparity greater than 0.5 are considered as "close" and those above are considered as "far".

The depth estimation error was measured using the following metrics: For close objects:

$$E_{d_c} = \frac{\sum_{i,j} (|d - d_{adv}| \odot M_f)[d > 0.5]}{\sum_{i,j} M_f[d > 0.5]} \quad (13)$$

For far objects:

$$E_{d_f} = \frac{\sum_{i,j} (|d - d_{adv}| \odot M_f)[d \leq 0.5]}{\sum_{i,j} M_f[d \leq 0.5]} \quad (14)$$

The ratio of affected region is measured as the ratio of pixels that their depth value has changed above a certain threshold depending on whether the object is classified as "close" or "far" with respect to the number of pixels in M_f . For close objects, any change in pixel's depth value above 0.1, that pixel is considered as affected. As for far objects, the change should be above 0.01. $\mathbf{I}(x)$ is the indicator function that evaluates to 1 only when the condition x is true. We distinguish two terms: For "close" objects

$$R_{a_c} = \frac{\sum_{i,j} \mathbf{I}((|d - d_{adv}| \odot M_f)[d > 0.5] > 0.1)}{\sum_{i,j} M_f[d > 0.5]} \quad (15)$$

for "far" objects:

$$R_{a_f} = \frac{\sum_{i,j} \mathbf{I}((|d - d_{adv}| \odot M_f)[d \leq 0.5] > 0.01)}{\sum_{i,j} M_f[d \leq 0.5]} \quad (16)$$

C. Evaluation Results

In order to assess the impact of the penalized depth loss, we use the monodepth2 as the victim MDE model. We run the patch for 4000 epochs. For the Adam optimizer, we use a learning rate of 0.01. A patch scale equal to 0.2 was applied. We first generate a patch by optimizing the conventional loss function and, as illustrated in Figure 3, the resulted affected region is restricted to the location of the patch, a slightly better performance than patches in [1], [2]. We later test with the modified depth loss defined in Section II-E. The resulting patch succeeded in completely hiding the entire object.

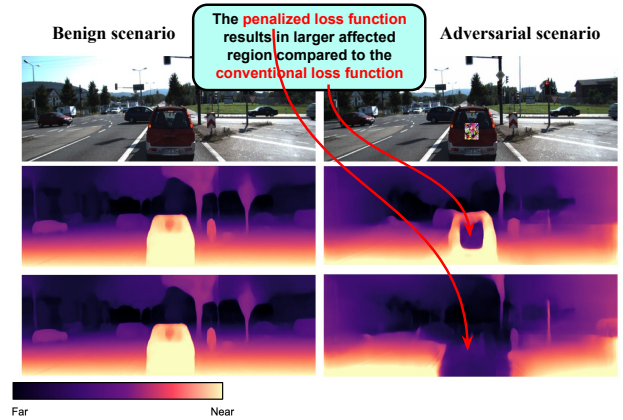


Fig. 3: Depth prediction w/o the penalized loss function: (Top) the input images, (Middle) results without the penalized depth loss (using the conventional loss), (Bottom) results with the penalized depth loss.

We also run our attack with the three MDE models and we target the two classes of objects for each model. First we generate an adversarial patch for pedestrians/cyclists with a patch scale equal to 0.2. As shown in Figure 4, our patch is effective and is capable of completely hiding the cyclist. Intuitively, relatively small objects are easier to hide or

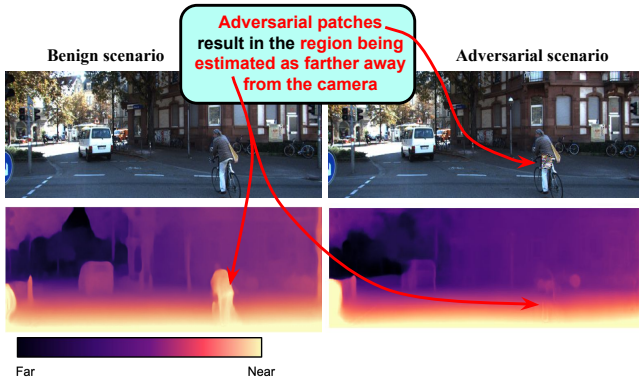


Fig. 4: Impact of APARATE on pedestrian/cyclist class.

change their depth, however, smaller objects require smaller patches and thereby relatively less effective ones.

For the second experiment, we generate an adversarial patch for the car class. We use the same patch scale 0.2. Almost all objects that are embedded with the APARATE patch were completely hidden whatever their shape, size and their distance from the camera. Which further proves the robustness of our proposed patch.

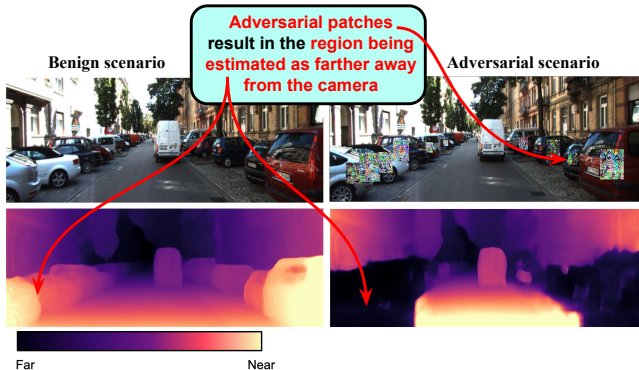


Fig. 5: Impact of APARATE on car class.

D. APARATE Performance

We evaluate the mean depth estimation errors E_{d_c} and E_{d_f} and the ratios of the affected regions R_{a_c} and R_{a_f} of the target object in 100 scenes from the KITTI dataset and take the average as the result.

TABLE I: Attack performance on "close" and "far" objects.

Models	E_{d_c}	R_{a_c}	E_{d_f}	R_{a_f}
Monodepth2	0.55	0.99	0.23	0.87
Depthhints	0.53	0.98	0.2	0.85
Manydepth	0.53	0.98	0.21	0.87

The obtained results can be interpreted as follows: Assuming that the farthest point captured by the camera is 100 meters away, objects in the range of [0, 50] meters, in accordance with our evaluation, are considered as "close", and those in the range of [50, 100] meters are considered as

"far". According to the results in Table II, when attacking a monodepth2-based MDE, our patch is capable of changing the depth of any object at a range of [0, 50] meters by an average of 55% and an average of 23% for any object at a range of [50, 100] meters. For instance, in an urban region scenario, for a car driving at a speed of 40 km/h, the brake distance should be more than 24 meters, it's the distance required for a car to be able to safely stop before hitting the other car. Using our patch, a car that is 20 meters away is predicted to be at a distance of more than 31 meters, which would result in a confirmed crash. As for In a high-way scenario: with a speed limit of 160 km/h, the safe distance is 96 meters. When using our patch, a car that is 90 meters far is predicted to be 110 meters away. This clearly illustrates the calamitous impact of the proposed attack. We also can notice that our patch results in more than 98% and 85% of the target region being affected for both close and far objects, respectively.

E. APARATE vs Existing Work

We ran experiments to quantitatively compare our attack to previous work [2] and [1]. We use the monodepth2 MDE model to evaluate the depth estimation error and The ratio of affected region. As shown in Table II, our proposed attack achieves the highest change in depth estimation and covers the largest area.

TABLE II: APARATE performance vs. existing attacks.

Attack	E_{d_c}	R_{a_c}	E_{d_f}	R_{a_f}
APARATE	0.55	0.99	0.23	0.87
Cheng et al. [2]	0.21	0.47	0.10	0.32
Yamanaka et al [1]	0.13	0.26	0.06	0.14

We also use the mean square error (MSE) to evaluate the model's performance with respect to the output depth map prediction of a clean input. This metric is defined below.

$$MSE = \frac{1}{n} \sum_{i=1}^n (\hat{y}_i - y_i)^2 \quad (17)$$

As illustrated in Table III, our attack achieves the highest error compared to other state of the art attacks.

TABLE III: MSE of adversarial example compared to the original images for different attacks.

Attack	APARATE	[2]	[1]
MSE	0.49	0.12	0.05

F. The Influence of Patch Scale

We evaluate our attack on a car object class with three different target patch sizes 0.1, 0.2, and 0.3. We use the three depth estimation models to assess the mean depth error and the ratio of the affected region. Tables IV and VI present the results of mean depth error of "close" and "far" objects, respectively. We can notice that E_d increases with the size

of the patch for all three target models. As expected, larger patches have a higher impact on the resulting depth error. Same trend can be noticed with the ratio of affected regions, see Tables V and VII, larger affected regions are paired with larger patches.

TABLE IV: E_{d_c} for different patch scales.

Scale	Monodepth2	Depthhints	Manydepth
0.1	0.46	0.37	0.3
0.2	0.55	0.53	0.53
0.3	0.66	0.64	0.63

TABLE V: R_{a_c} for different patch scales.

Scale	Monodepth2	Depthhints	Manydepth
0.1	0.97	0.95	0.97
0.2	0.99	0.98	0.98
0.3	0.99	0.99	0.99

TABLE VI: E_{d_f} for different patch scales.

Scale	Monodepth2	Depthhints	Manydepth
0.1	0.14	0.11	0.09
0.2	0.23	0.2	0.21
0.3	0.34	0.31	0.32

TABLE VII: R_{a_f} for different patch scales.

Scale	Monodepth2	Depthhints	Manydepth
0.1	0.84	0.82	0.82
0.2	0.87	0.85	0.87
0.3	0.89	0.87	0.88

IV. DISCUSSION

To evaluate the robustness of our patch to existing defenses, we use 3 off the shelf defense techniques that perform input transformations without re-training the victim models. We perform JPEG compression [29], adding Gaussian noise [30], median blurring [31]. We report the mean depth error of the benign scenarios, i.e., when applying the defense technique on the benign images (E_{d_B}) and of the adversarial scenario, i.e., when applying the defense on the adversarial image (E_{d_c}). We notice that our patch is still effective even when using a defense technique (See Tables VIII, IX, and X). Even though the applied defenses resulted in a drop in the mean error depth, our patch still resulted in an average of 0.2 meaning over 5 meters error in depth prediction, except for the median blur which already significantly degrades the baseline performance of the MDE network.

V. RELATED WORK

In autonomous driving, prior work focused on perception sensor security. In fact, many attacks were proposed with the purpose of jamming cameras [32]–[34], GPS [35], LiDAR

TABLE VIII: Mean depth error when applying JPEG compression.

Parameters	90	70	50	30
E_{d_c}	0.23	0.22	0.19	0.15
E_{d_B}	0	0	0.001	0.001

TABLE IX: Mean depth error when applying median blur.

Parameters	5	10	15	20
E_{d_c}	0.13	0.12	0.13	0.15
E_{d_B}	0.09	0.08	0.06	0.08

TABLE X: Mean depth error when applying Gaussian noise.

Parameters	0.01	0.02	0.05	0.1
E_{d_c}	0.24	0.21	0.2	0.21
E_{d_B}	0.01	0.03	0.05	0.089

[36], [37], RADAR [38], ultrasonic [32] and IMU [39], [40]. Some other works, proposed attacks for regression tasks (e.g., optical flow estimation [41] and depth estimation [1]), and others focused on classification tasks (e.g., 2D object detection and classification [42], [43], tracking [44], traffic light detection [45], and lane detection [46]). In this work, we focus on jamming MDE models.

Unlike existing physical attacks that have targeted tasks such as object detection [22], [47], image classification [42], [48], face recognition [49], [50], attacks on depth estimation has received scarce attention. Zhang [51] proposes an attack technique to enhance the performance in the universal attack scenario. Wong [52] proposes a strategy to generate targeted adversarial perturbation on images and randomly change the depth map. These two attacks focus on digital perturbations and therefore are not suitable to the physical world. Yamanaka [1] proposes a method to generate printable adversarial patches but the patch was trained for random locations on the scene. Cheng [2] has focused on the stealthiness of the produced patch and making sure that the generated patch is not conspicuous and attention grabbing. The problem with the generated patch is its an object specific patch, i.e, one needs to separately retrain the patch for each target object. The patch also suffered from the limited affected region and was trained for a specific setting; a fixed distance between the object and the camera, which makes the patch ineffective for other distances.

Different from prior efforts, we focus on the impact of the produced patch, making sure that it covers the whole target object to ensure a complete deception of the DNN-based vision system. We propose a framework that grants the effectiveness of the patch on any object of the same class with different shapes and sizes. Our patch also works for different distances between the object where it is placed and the vision system camera.

VI. CONCLUSION

In this paper, we propose a physical adversarial patch named APARATE crafted with the aim of jeopardizing MDE-based vision systems. APARATE is an adversarial patch capable of fully hiding objects or altering their depth in a given scene regardless of their size, shape or location. We experimentally prove the effectiveness and robustness of our patch for different target objects. Our patch achieves more than 14 *meters* mean depth estimation error, with 99% of the target region being affected. Our patch also showed robustness against input transformations-based defense techniques. The impact of the proposed attack could bring great damage, loss, destruction and devastation to life and properties. We think that this should alert the community and motivate investigating more robust and adaptive defenses.

REFERENCES

- [1] K. Yamanaka, R. Matsumoto, K. Takahashi, and T. Fujii, "Adversarial patch attacks on monocular depth estimation networks," *IEEE Access*, vol. 8, pp. 179 094–179 104, 2020.
- [2] Z. Cheng, J. Liang, H. Choi, G. Tao, Z. Cao, D. Liu, and X. Zhang, "Physical attack on monocular depth estimation with optimal adversarial patches," 2022. [Online]. Available: <https://arxiv.org/abs/2207.04718>
- [3] X. Yang, J. Chen, Y. Dang, H. Luo, Y. Tang, C. Liao, P. Chen, and K.-T. Cheng, "Fast depth prediction and obstacle avoidance on a monocular drone using probabilistic convolutional neural network," *IEEE Transactions on Intelligent Transportation Systems*, vol. 22, no. 1, pp. 156–167, 2021.
- [4] Y. Wang, W.-L. Chao, D. Garg, B. Hariharan, M. Campbell, and K. Q. Weinberger, "Pseudo-lidar from visual depth estimation: Bridging the gap in 3d object detection for autonomous driving," in *2019 IEEE/CVF Conference on Computer Vision and Pattern Recognition (CVPR)*, 2019, pp. 8437–8445.
- [5] K. Tateno, F. Tombari, I. Laina, and N. Navab, "Cnn-slam: Real-time dense monocular slam with learned depth prediction," *2017 IEEE Conference on Computer Vision and Pattern Recognition (CVPR)*, pp. 6565–6574, 2017.
- [6] F. Wimbauer, N. Yang, L. von Stumberg, N. Zeller, and D. Cremers, "Monorec: Semi-supervised dense reconstruction in dynamic environments from a single moving camera," in *2021 IEEE/CVF Conference on Computer Vision and Pattern Recognition (CVPR)*, 2021, pp. 6108–6118.
- [7] L. von Stumberg, P. Wenzel, N. Yang, and D. Cremers, "Lm-reloc: Levenberg-marquardt based direct visual relocalization," *CoRR*, vol. abs/2010.06323, 2020. [Online]. Available: <https://arxiv.org/abs/2010.06323>
- [8] "Andrej karpathy - ai for full-self driving at tesla," <https://youtu.be/hx7BXih7zx8>, accessed: March 1, 2023.
- [9] "Tesla ai day 2021," <https://www.youtube.com/live/j0z4FweCy4M?feature=share>, accessed: March 1, 2023.
- [10] V. Guizilini, R. Ambrus, S. Pillai, and A. Gaidon, "Packnet-sfm: 3d packing for self-supervised monocular depth estimation," *CoRR*, vol. abs/1905.02693, 2019. [Online]. Available: <http://arxiv.org/abs/1905.02693>
- [11] S. Aich, J. M. U. Vianney, M. A. Islam, M. Kaur, and B. Liu, "Bidirectional attention network for monocular depth estimation," *CoRR*, vol. abs/2009.00743, 2020. [Online]. Available: <https://arxiv.org/abs/2009.00743>
- [12] I. J. Goodfellow, J. Shlens, and C. Szegedy, "Explaining and harnessing adversarial examples," 2014.
- [13] N. Carlini and D. A. Wagner, "Towards evaluating the robustness of neural networks," *CoRR*, vol. abs/1608.04644, 2016. [Online]. Available: <http://arxiv.org/abs/1608.04644>
- [14] A. Kurakin, I. J. Goodfellow, and S. Bengio, "Adversarial examples in the physical world," *CoRR*, vol. abs/1607.02533, 2016. [Online]. Available: <http://arxiv.org/abs/1607.02533>
- [15] I. Evtimov, K. Eykholt, E. Fernandes, T. Kohno, B. Li, A. Prakash, A. Rahmati, and D. Song, "Robust physical-world attacks on machine learning models," *CoRR*, vol. abs/1707.08945, 2017. [Online]. Available: <http://arxiv.org/abs/1707.08945>
- [16] V. Venceslai, A. Marchisio, I. Alouani, M. Martina, and M. Shafique, "Neuroattack: Undermining spiking neural networks security through externally triggered bit-flips," 2020.
- [17] A. Kurakin, I. J. Goodfellow, and S. Bengio, "Adversarial examples in the physical world," *CoRR*, vol. abs/1607.02533, 2016. [Online]. Available: <http://arxiv.org/abs/1607.02533>
- [18] D. P. Kingma and J. Ba, "Adam: A method for stochastic optimization," 2014. [Online]. Available: <https://arxiv.org/abs/1412.6980>
- [19] Z. Jiang, L. Zhao, S. Li, and Y. Jia, "Real-time object detection method based on improved yolov4-tiny," *CoRR*, vol. abs/2011.04244, 2020. [Online]. Available: <https://arxiv.org/abs/2011.04244>
- [20] T.-Y. Lin, M. Maire, S. J. Belongie, J. Hays, P. Perona, D. Ramanan, P. Dollár, and C. L. Zitnick, "Microsoft coco: Common objects in context," in *ECCV*, 2014.
- [21] Y.-C.-T. Hu, J.-C. Chen, B.-H. Kung, K.-L. Hua, and D. S. Tan, "Naturalistic physical adversarial patch for object detectors," in *2021 IEEE/CVF International Conference on Computer Vision (ICCV)*, 2021, pp. 7828–7837.
- [22] S. Thys, W. V. Ranst, and T. Goedemé, "Fooling automated surveillance cameras: adversarial patches to attack person detection," *CoRR*, vol. abs/1904.08653, 2019. [Online]. Available: <http://arxiv.org/abs/1904.08653>
- [23] C. Godard, O. M. Aodha, and G. J. Brostow, "Digging into self-supervised monocular depth estimation," *CoRR*, vol. abs/1806.01260, 2018. [Online]. Available: <http://arxiv.org/abs/1806.01260>
- [24] J. Watson, M. Firman, G. Brostow, and D. Turmukhambetov, "Self-supervised monocular depth hints," in *2019 IEEE/CVF International Conference on Computer Vision (ICCV)*, 2019, pp. 2162–2171.
- [25] J. Watson, O. M. Aodha, V. Prisacariu, G. Brostow, and M. Firman, "The temporal opportunist: Self-supervised multi-frame monocular depth," in *2021 IEEE/CVF Conference on Computer Vision and Pattern Recognition (CVPR)*. Los Alamitos, CA, USA: IEEE Computer Society, jun 2021, pp. 1164–1174. [Online]. Available: <https://doi.ieeecomputersociety.org/10.1109/CVPR46437.2021.00122>
- [26] K. He, X. Zhang, S. Ren, and J. Sun, "Deep residual learning for image recognition," in *2016 IEEE Conference on Computer Vision and Pattern Recognition (CVPR)*, 2016, pp. 770–778.
- [27] J. Deng, W. Dong, R. Socher, L.-J. Li, K. Li, and L. Fei-Fei, "Imagenet: A large-scale hierarchical image database," in *2009 IEEE Conference on Computer Vision and Pattern Recognition*, 2009, pp. 248–255.
- [28] A. Geiger, P. Lenz, and R. Urtasun, "Are we ready for autonomous driving? the kitti vision benchmark suite," in *2012 IEEE Conference on Computer Vision and Pattern Recognition*, 2012, pp. 3354–3361.
- [29] G. K. Dziugaite, Z. Ghahramani, and D. M. Roy, "A study of the effect of JPG compression on adversarial images," *CoRR*, vol. abs/1608.00853, 2016. [Online]. Available: <http://arxiv.org/abs/1608.00853>
- [30] Y. Zhang and P. Liang, "Defending against whitebox adversarial attacks via randomized discretization," in *Proceedings of the Twenty-Second International Conference on Artificial Intelligence and Statistics*, ser. Proceedings of Machine Learning Research, K. Chaudhuri and M. Sugiyama, Eds., vol. 89. PMLR, 16–18 Apr 2019, pp. 684–693. [Online]. Available: <https://proceedings.mlr.press/v89/zhang19b.html>
- [31] W. Xu, D. Evans, and Y. Qi, "Feature squeezing: Detecting adversarial examples in deep neural networks," *CoRR*, vol. abs/1704.01155, 2017. [Online]. Available: <http://arxiv.org/abs/1704.01155>
- [32] C. Yan, "Can you trust autonomous vehicles : Contactless attacks against sensors of self-driving vehicle," 2016.
- [33] B. Nassi, Y. Mirsky, D. Nassi, R. Ben-Netanel, O. Drokin, and Y. Elovici, "Phantom of the adas: Securing advanced driver-assistance systems from split-second phantom attacks," in *Proceedings of the 2020 ACM SIGSAC Conference on Computer and Communications Security*, ser. CCS '20. New York, NY, USA: Association for Computing Machinery, 2020, p. 293–308. [Online]. Available: <https://doi.org/10.1145/3372297.3423359>
- [34] J. Petit, B. Stottelaar, and M. Feiri, "Remote attacks on automated vehicles sensors : Experiments on camera and lidar," 2015.

- [35] J. Shen, J. Y. Won, Z. Chen, and Q. A. Chen, "Drift with devil: Security of Multi-Sensor fusion based localization in High-Level autonomous driving under GPS spoofing," in *29th USENIX Security Symposium (USENIX Security 20)*. USENIX Association, Aug. 2020, pp. 931–948. [Online]. Available: <https://www.usenix.org/conference/usenixsecurity20/presentation/shen>
- [36] Y. Cao, C. Xiao, B. Cyr, Y. Zhou, W. Park, S. Rampazzi, Q. A. Chen, K. Fu, and Z. M. Mao, "Adversarial sensor attack on lidar-based perception in autonomous driving," ser. CCS '19. New York, NY, USA: Association for Computing Machinery, 2019, p. 2267–2281. [Online]. Available: <https://doi.org/10.1145/3319535.3339815>
- [37] H. Shin, D. Kim, Y. Kwon, and Y. Kim, "Illusion and dazzle: Adversarial optical channel exploits against lidars for automotive applications," Cryptology ePrint Archive, Paper 2017/613, 2017, <https://eprint.iacr.org/2017/613>. [Online]. Available: <https://eprint.iacr.org/2017/613>
- [38] A. Guesmi and I. Alouani, "a-rna: Adversarial radio noise attack to fool radar-based environment perception systems," 2022. [Online]. Available: <https://arxiv.org/abs/2211.01112>
- [39] Y. Tu, Z. Lin, I. Lee, and X. Hei, "Injected and delivered: Fabricating implicit control over actuation systems by spoofing inertial sensors," in *27th USENIX Security Symposium (USENIX Security 18)*. Baltimore, MD: USENIX Association, Aug. 2018, pp. 1545–1562. [Online]. Available: <https://www.usenix.org/conference/usenixsecurity18/presentation/tu>
- [40] T. Trippel, O. Weisse, W. Xu, P. Honeyman, and K. Fu, "Walnut: Waging doubt on the integrity of mems accelerometers with acoustic injection attacks," in *2017 IEEE European Symposium on Security and Privacy (EuroS&P)*, 2017, pp. 3–18.
- [41] A. Ranjan, J. Janai, A. Geiger, and M. J. Black, "Attacking optical flow," *CoRR*, vol. abs/1910.10053, 2019. [Online]. Available: <http://arxiv.org/abs/1910.10053>
- [42] K. Eykholt, I. Evtimov, E. Fernandes, B. Li, A. Rahmati, F. Tramèr, A. Prakash, T. Kohno, and D. Song, "Physical adversarial examples for object detectors," in *Proceedings of the 12th USENIX Conference on Offensive Technologies*, ser. WOOT'18. USA: USENIX Association, 2018, p. 1.
- [43] T. B. Brown, D. Mané, A. Roy, M. Abadi, and J. Gilmer, "Adversarial patch," *CoRR*, vol. abs/1712.09665, 2017. [Online]. Available: <http://arxiv.org/abs/1712.09665>
- [44] Y. Jia, Y. Lu, J. Shen, Q. A. Chen, H. Chen, Z. Zhong, and T. Wei, "Fooling detection alone is not enough: Adversarial attack against multiple object tracking," in *ICLR*, 2020.
- [45] R. Duan, X. Ma, Y. Wang, J. Bailey, A. K. Qin, and Y. Yang, "Adversarial camouflage: Hiding physical-world attacks with natural styles," in *2020 IEEE/CVF Conference on Computer Vision and Pattern Recognition (CVPR)*. Los Alamitos, CA, USA: IEEE Computer Society, jun 2020, pp. 997–1005. [Online]. Available: <https://doi.ieeecomputersociety.org/10.1109/CVPR42600.2020.00108>
- [46] T. Sato, J. Shen, N. Wang, Y. J. Jia, X. Lin, and Q. A. Chen, "Hold tight and never let go: Security of deep learning based automated lane centering under physical-world attack," *CoRR*, vol. abs/2009.06701, 2020. [Online]. Available: <https://arxiv.org/abs/2009.06701>
- [47] Y.-C.-T. Hu, J.-C. Chen, B.-H. Kung, K.-L. Hua, and D. S. Tan, "Naturalistic physical adversarial patch for object detectors," in *2021 IEEE/CVF International Conference on Computer Vision (ICCV)*, 2021, pp. 7828–7837.
- [48] A. Athalye, L. Engstrom, A. Ilyas, and K. Kwok, "Synthesizing robust adversarial examples," in *ICML*, 2018.
- [49] M. Sharif, S. Bhagavatula, L. Bauer, and M. K. Reiter, "Accessorize to a crime: Real and stealthy attacks on state-of-the-art face recognition," in *Proceedings of the 2016 ACM SIGSAC Conference on Computer and Communications Security*, ser. CCS '16. New York, NY, USA: Association for Computing Machinery, 2016, p. 1528–1540. [Online]. Available: <https://doi.org/10.1145/2976749.2978392>
- [50] S. Komkov and A. Petiushko, "Advhat: Real-world adversarial attack on arcface face id system," in *2020 25th International Conference on Pattern Recognition (ICPR)*. Los Alamitos, CA, USA: IEEE Computer Society, jan 2021, pp. 819–826. [Online]. Available: <https://doi.ieeecomputersociety.org/10.1109/ICPR48806.2021.9412236>
- [51] Z. Zhang, X. Zhu, Y. Li, X. Chen, and Y. Guo, "Adversarial attacks on monocular depth estimation," *CoRR*, vol. abs/2003.10315, 2020. [Online]. Available: <https://arxiv.org/abs/2003.10315>
- [52] A. Wong, S. Cicek, and S. Soatto, "Targeted adversarial perturbations for monocular depth prediction," in *Proceedings of the 34th International Conference on Neural Information Processing Systems*, ser. NIPS'20. Red Hook, NY, USA: Curran Associates Inc., 2020.